FINAL REPORT

on

Contract NAS8-30624

A STUDY OF A PLUME INDUCED SEPARATION SHOCK WAVE, INCLUDING EFFECTS OF PERIODIC PLUME UNSTEADINESS

by

Julian O. Doughty, Principal Investigator

Prepared for

National Aeronautics and Space Administration
George C. Marshall Space Flight Center
Marshall Space Flight Center, Alabama 35812

October 1976

BER Report No. 207-02

FINAL REPORT

on

Contract NAS8-30624

A STUDY OF A PLUME INDUCED SEPARATION SHOCK WAVE, INCLUDING EFFECTS OF PERIODIC PLUME UNSTEADINESS

by

Julian O. Doughty, Principal Investigator

Prepared for

National Aeronautics and Space Administration
George C. Marshall Space Flight Center
Marshall Space Flight Center, Alabama 35812

October 1976

BER Report No. 207-02

ABSTRACT

A wind tunnel investigation was conducted to study the flow field in which separation is caused by an expaning plume, with emphasis on effects associated with periodic unsteadiness in the plume. The separation shock was photographed with high speed motion pictures, from which mean shock position and excursion data are reported. Pressure fluctuations were measured beneath the separation shock and statistics of the results are reported. A response of the separation shock to plume periodic unsteadiness was identified, and the magnitude of a corresponding transfer function was defined and is reported. Also, small harmonic effects in plume response to periodic unsteadiness were noted.

The stabilizing effect of a lateral surface protuberance near the separation shock wave was investigated. The protuberance configuration was a lateral circular cylinder, and various diameters, all less than the boundary layer thickness, were employed.

Comparisons of normalized power spectrum correlation using boundary layer thickness and separation length as the pertinent length are illustrated. A brief discussion of the scaling considerations for the pressure statistics associated with plume induced flow separation is given.

TABLE OF CONTENTS

LIST OF FIGURES

LIST OF SYMBOLS

a	speed of sound, m/sec
c_p	specific heat at constant pressure, kJ/kg-K
E	Eckert number
f	frequency, H_z
F	plume pulse forcing function, atm^2
G	power spectral density, atm^2-sec
$\bar{G}$	Grashof number
$\|H(f)\|$	transfer function magnitude
k	thermal conductivity, w/m-k
L	distance measured from mean shock location, cm
L, L_1, L_2	characteristic lengths, cm
M	Mach number
P	pressure, atm
$\bar{P}$	Prandtl number
q	dynamic pressure, atm
r^*	dimensionless position vector
R	Reynolds number or shock spectrum response to plume pulsing, atm^2
t	time, sec
t^*	dimensionless time
t_o	time period for statistical integration, sec
T	temperature, K
u, v, w	velocity components, m/sec
U	freestream velocity, m/sec
x	separation shock location, cm
$\bar{x}$	mean separation shock location, cm

δ	boundary layer thickness, cm
θ	separation shock angle, deg
μ	viscosity, N-sec/m^2
ρ	density, kg/m^3
σ	standard deviation of separation shock positions, cm
τ	time, sec

Subscripts

m	model
p	prototype
rms	root-mean-square
∞	freestream variable

INTRODUCTION

A rocket booster vehicle will typically produce a significantly underexpanded engine exhaust in the latter duration of its burn. In that condition, the exhaust plumes to a large diameter and alters the vehicle flow field considerably by generating a separated flow region which engulfs the aft end of the vehicle. The vehicle boundary layer separates well forward of the plume itself, and a separation shock wave radiates from a position near the separation point. The flow field is illustrated in Figure 1.

An inherent unsteadiness exists for the separated flow as is often experienced with rigid surface compression corner flow at large Reynolds numbers. (For example, see references 1,2,3 and 4.) Separation shock excursions of several meters were reported by Jones from in-flight observations of a Saturn V vehicle [5]*. One would expect rather severe surface pressure fluctuations to accompany such shock motion, and significantly, the engine plume is usually large at the altitude where the vehicle encounters maximum dynamic pressure.

Large liquid fuel rocket engines exhibit a periodic unsteadiness, therefore, the effect of that unsteadiness on the plume induced flow field is of concern. This report experimentally examines the plume induced flow field with and without periodic plume unsteadiness. Data are reported for an axisymmetric body at Mach 2.9 with a cold air plume generated by secondary flow.

*Numbers in brackets refer to references in the List of References at the end of this report.

Data are also reported which examine the effect of lateral surface protuberances, immersed in the boundary layer, near the induced boundary separation. The objective is to suppy data which are useful in assessing the possibility of reducing surface pressure fluctuations by capturing the separation shock.

MODEL AND TEST FACILITIES

Model Description

The basic configuration of the model used in this study is a cone-cylinder body which produces a plume near the aft end. The plume is produced from a secondary supply of air with a maximum working pressure of 136 atm. A photograph of the model is shown in Figure 2.

The basic model is identical to that used for previous tests [6,7], and is mounted on the wind tunnel wall with its axis of symmetry located at the tunnel wall boundary layer displacement thickness. The wall mounting arrangement allows easier access for the plume generation flow and allows a larger diameter body to be used as compared with a sting mount. Locating the model on the wall boundary layer displacement thickness simulates true axisymmetric flow. This was verified during earlier tests with this model [6]. The model details and dimensions are given in Figure 3.

Stainless steel fins are used on the model to isolate the test flow from the tunnel wall effect and preserve axisymmetric flow in a circular sector where data are taken. The fins are 1/16 inch thick and have a 10^{o} half wedge cut in the lower surface of the leading edge. A flat plate is seen by the flow on the upper surface. The leading edge is swept 70^{o} to maintain a minimum distance from the leading edge to the separated region, minimizing the effect of the fin boundary layer.

Plume Generation

The plume producing portion of the model is detailed in Figure 4. The plume nozzle is composed of two conical surfaces with a common apex located on the model axis of symmetry. It is designed for an isentropic exit Mach number 2.94. The model fins extend into the plume nozzle to preserve symmetry within a circular sector.

Plume Pulsing

Plume unsteadiness (or pulsing) is generated by the apparatus detailed in Figures 4 and 5. The unsteadiness is generated by periodically diverting a part of the plume supply air to the atmosphere. This is accomplished with a variable speed rotating disk with evenly spaced holes on a circumference. The holes align with a teflon orifice which is teed off the plume air supply. Pulse frequency is controlled by the disk rotational speed, and the pulse magnitude is controlled by the orifice size.

The nature of the pressure signal, measured in the plume settling chamber, is that of a periodic component superimposed on a larger steady component. The periodic part is approximately a sine wave, especially for cases in which the orifice size is about the same as the disk holes. The wave is somewhat like a "flattened sine wave" for tests in which the orifice is considerably smaller than the disk holes.

The time required for a pulse to travel from the orifice to the plume settling chamber places an upper limit on the frequency for which a good pressure signal can be generated. In this experiment the distance from the orifice to the settling chamber is approximately 10 cm, and wave distortion is evident at frequencies above 500 or 600 Hz. At 1000 Hz the distortion is severe. A periodic wave is produced, but with a greatly reduced amplitude and an appearance more like a rectified sine wave. It is assumed that at

very high frequencies individual pulses interfere with each other. Data reported here are for frequencies well below the distortion range.

Wind Tunnel

The wind tunnel used in this project is a blowdown supersonic tunnel with a 16 by 16 cm test section, located at The University of Alabama, Tuscaloosa. A major part of the data collection and reduction was done by Messers J.D. Dagen and F.L. Smith.

Test Conditions

All data reported are for the following freestream conditions:

Mach no. = 2.9

airspeed = 607 m/sec

stagnation temperature = 288 to 294 K

static pressure = 0.151 atm

stagnation pressure = 4.76 atm

dynamic pressure = 0.878 atm

Reynolds no. = 4.9×10^7 per meter.

The plume stagnation pressure was nominally 33 atm. That value located the mean position of the separation shock on the surface pressure transducer and generated a characteristic signal which could readily be identified on an oscilliscope. Small adjustments in stagnation pressure were necessary to produce that condition in the various tests.

SEPARATION SHOCK WAVE EXCURSIONS

Test Procedure

The separation shock was photographed with a Schlieren system projecting into a high speed camera. The tests were made at a camera speed of about 800 frames per second and an exposure time of about 0.002 seconds. Previous experience had indicated that greater exposure times would not "freeze" the

shock motion. Measurements of shock direction and position were taken from the film by single frame projection onto a grid. The task was simplified by the fact that the shock direction remained essentially constant during the shock motion.

Results

Observation and measurement from the high speed motion pictures showed that the separation shock was in constant motion, regardless of whether or not there was plume pulsing. As it moved it maintained essentially a constant shock angle with the freestream. In these tests, the shock angle was 28 degrees and mean shock location, $\bar{x}$, was 5.87 cm. In this context, shock location and separation length are taken to be the same. Histograms of shock excursion for a steady plume and for four different pulsing frequencies are shown in Figure 6. Each histogram represents 4,000 measured positions. For the tests involving an unsteady plume, the plume pressure pulses (RMS) were 4.3 percent of the plume stagnation pressure.

There are no distinctions among the histograms which could not be attributed to experimental error and the finite data sample. The magnitude of plume pulsing used was sufficient to produce obvious distinctions in the surface pressure power spectra associated with the separation shock excursions (to be discussed later). Therefore, if any effect exists, of plume unsteadiness on the shock excursion histogram, it is rather subtle.

The motion pictures of shock travel were viewed at several different frame speeds. It was not possible to distinguish the effect of plume pulsing in this manner. In all instances the impression from viewing movement of the shock was that it jumps from one position of momentary stability to another in an apparently random manner.

SEPARATION SHOCK WAVE SURFACE PRESSURES

Test Procedure

Surface pressure fluctuations at the separation shock were measured by a flush mounted strain gage type transducer with a diameter of 2 mm and a natural frequency above 100 kHz. The static pressure level was eliminated by feeding the pressure from a surface orifice, located laterally adjacent to the transducer, through a 3 m length of tubing to the reverse side of the transducer diaphram. The length of tubing filtered the fluctuations and provided a time-average reference so that the transducer sensed only the pressure fluctuations. This technique was suggested by Mr. L. Muhlstein, Jr., of Ames Research Center, who was also kind enough to supply filtering data.

Plume pressure fluctuations were measured by a piezoelectric transducer located in the plume settling chamber. All fluctuating pressure data were stored on magnetic tape for subsequent reduction.

Data Processing

Surface pressure fluctuations at the separation shock, were processed to yield root-mean-square levels and power spectral densities. The power spectra were obtained from a one-third octave analysis using a Bruel and Kjaer 2121 signal analyzer. This instrument was used to filter the input signal except for that in a selected bandwidth, and it gave the root-mean-square level for that bandwidth averaged over a selected period (10 seconds in this case). The taped signal was repeatedly input at different filter selections until the significant frequency spectrum had been swept. The output (see Figure 7 for examples) was then in an ideal condition to be processed into a one-third octave power spectrum. Broadband root-mean-square levels were obtained in the same manner, except that no filtering of the signal was used.

For purposes of determining the level of the plume pressure pulse signal,

it was desired to separate the periodic part from background produced by turbulence in the plume settling chamber. The signal was autocorrelated, producing essentially a sine wave with constant amplitude except for the zero-time amplitude which was somewhat greater. (The zero-time amplitude represents the mean-square value of the entire signal. However, the background noise quickly "washes out".) Then the final amplitude of the autocorrelation was taken to be the mean-square value of the periodic plume pressure. In most tests the pulse signal was considerably greater than the background turbulence, and it was only in tests involving a very low magnitude of plume pulsing that the correlation technique was necessary, but it was done in all cases for consistency.

One of the most obvious effects of periodic plume unsteadiness is the generation of a spike on the power spectrum of the surface pressure beneath the separation shock. The spike is located at the plume pulse frequency. For the purpose of quantitatively relating periodic plume unsteadiness to the separation shock response, plume forcing magnitude and the spectrum response are defined. Plume forcing magnitude is defined to be the root-mean-square level of the pulsing signal measured as described in the last paragraph. The spectrum response is defined to be the strength of the spike produced, measured in the following manner: the area under the spectrum spike which is above the balance of the spectrum with the spike faired out. In determining the area under the spike, each one-third octave band produces a rectangular area consistent with the filter process by which the spectrum is produced. The quantities identified as "forcing" and "response" are clearly not the only ones which could have been chosen. Since there is some arbitrariness, the "best" definitions will likely vary according to personal preference and situation. However, it is hoped that the definitions selected are reasonable

and useful.

Results

Figure 7 shows the pressure signals as taken directly from the one-third octave filtering system. It compares the basic shock spectrum with the spectrum produced by a shock associated with periodic plume pulsing at 80 Hz and a magnitude of 3.76 percent of the plume stagnation pressure. The broadband level of the basic spectrum (steady plume) is 166.6 dB and that of the spectrum associated with plume unsteadiness is 166.9 dB. These spectra were produced by an ensemble average of eight different tests, for the basic spectrum, and ten different tests, for the unsteady plume generated spectrum. The intent was to reduce the data scatter and produce spectra in the rawest form possible, which incorporated no curve fairing or interpretation, for the purpose of examining the effect of the spike on the balance of the spectrum. Since the broadband levels of the spectra, with and without plume unsteadiness, are the same within experimental error (and this has been observed repeatedly in the course of this investigation), it appeared that the spike was produced at the expense of the balance of the spectrum. An examination of Figure 7 shows this to be the case, since the spectrum levels associated with plume pulsing are everywhere lower, except at the spike. The same data are shown in Figure 8 reduced as suggested by Coe [1], with the exception that Coe measured boundary layer thickness just ahead of the shock, whereas in this case it was measured at the mean shock location, but in the absence of a plume and consequently a separation shock. For the data, $\delta = 0.53$ cm.

With the definitions for forcing and response as previously stated, the response to periodic plume unsteadiness is displayed in Figure 9. Within experimental error, over the range tested, a linear relationship exists which is independent of pulse frequency. The results can be expressed in terms of a

transfer function if it is postulated that forcing and response are reasonably represented by a linear differential equation. Then the magnitude of the transfer function is

$$|H(f)| = \sqrt{\frac{R(f)}{F(f)}} = 0.0169 \qquad (16 \text{ Hz} \leq f \leq 250 \text{ Hz}),$$

and is constant for these data.

SHOCK STABILIZATION

Test Procedure

A series of tests were conducted to determine the effectiveness of a lateral protuberance in stabilizing a separation shock. The protuberances were circular cylinders wrapped around the model perpendicular to the flow direction. (See Figure 10.) The cylinders ranged in size from 0.158 cm to 0.406 cm in a boundary layer with a thickness of 0.53 cm.

To determine the effectiveness, the protuberances were located at various positions near the undisturbed mean shock location. For each location, twenty Schlieren photographs were made, from which the degree of stabilization was taken as being indicated by the standard deviation of the movement of the foot of the shock. The results should also be representative of the condition in which the mean shock position varies due to a changing pressure ratio between the plume stagnation and the freestream pressure because the separation shock angle (and thus the shock strength) is almost constant with respect to mean shock location (see reference 6).

Fluctuating pressure measurements were also made for the flow field near the protuberance. Root-mean-square pressure levels and power spectra were extracted from these measurements in the same manner as that described for previous tests. These results also are indicative of the effectiveness of shock stabilization.

Results

It was found that the activity of the separation shock could be reduced by a protuberance over a range of locations. To represent this it was necessary to define stabilization. The nature of the loss of stabilization, with increasing separation between original shock location and protuberance, was very different according to whether the protuberance was ahead of or behind the original shock location ($\bar{x}$). If the protuberance was ahead of the original shock location, loss of stabilization was clearly indicated by the sudden appearance of a shock, located behind the protuberance. However, loss of stabilization was a gradual process when the protuberance was behind the original shock location. Since loss of stabilization could easily be identified in the former case, the standard deviation of the movement of the foot of the shock for that case was taken as the limit of stabilization for the latter case also. The standard deviation of the shock movement for difference protuberance locations is given in Figure 11. The resulting zone of stabilization is shown in Figure 12. Additional information about the effectiveness is provided in Figure 13 which gives RMS pressure levels near a 0.26 cm diameter protuberance, with and without plume pulsing. Selected raw spectra for several of the locations are shown in Figures 14 and 15. The maximum RMS pressure level is down about 4 dB from the unstabilized condition, and the region of high level fluctuations is restricted. The high levels are not affected by plume pulsing, however, the levels behind the protuberance are considerably elevated by pulsing. It is interesting that the spectrum spike produced behind the protuberance is greater in magnitude than that produced by the stabilized shock. (See Figure 15.)

SCALING CONSIDERATIONS

With Geometric Similarity

The scaling laws for the statistics of pressure fluctuations can be stated rather directly for the case in which geometrically similar bodies are considered, and the statistics are not time varying. The governing equations are the continuity equation, the Navier-Stokes equations, the energy equation and appropriate ideal gas state equations. The variables taken as being dependent are usually, u,v,w,p,ρ and T, with the independent variables being the spatial coordinates and time. With selected reference quantities: U, ρ_∞, T_∞ and L, the equations may be expressed in terms of dimensionless variables with the pertinent flow parameters, necessary for similitude, appearing as coefficients of terms in the equations. For example, see reference 8, Chapter XII.

The requirement for flow field similarity for compressible flow of an ideal gas is the matching of the dimensionless parameters: Reynolds number, Mach number, Prandtl number, Grashof number and Eckert number, or the equivalent of that. Aside from the ideal gas assumption, the analysis, as stated, is further restricted by the assumption that temperature variations are mild enough that representative constant values of c_p, μ, and k can be used.

The previous statements lead to a functional form for any quantity which is dependent only on the flow field variables. For instance, the pressure, normalized to flow quantities, can be expressed

$$\frac{P}{\frac{1}{2}\rho_\infty U^2} = f_1(r^*, t^*, R, \bar{P}, \bar{G}, E) \qquad (1)$$

where r^* is a dimensionless position vector and t^* is a dimensionless time.

For the flows of interest, the Grashof number, $\bar{G}$, is unimportant since it reflects free convection effects. Also, the Eckert number, E, can usually be represented by the more commonly used Mach number, M, (again, see reference 8, Chapter XII). Then:

$$\frac{p}{\frac{1}{2}\rho_\infty U^2} = f_2\ (r^*,\ t^*,\ R,\ \bar{P},\ M). \tag{2}$$

The quantity P_{rms} is determined as:

$$P_{rms} = \left[\underset{t_o \to \infty}{\text{limit}}\ \frac{1}{t_o}\int_o^{t_o} p^2\ dt,\right]^{1/2}. \tag{3}$$

Then,

$$\frac{P_{rms}}{q} = f_3\ (r^*,\ R,\ \bar{P},\ M). \tag{4}$$

Finally, if attention is restricted to a single gas, and conditions are such as to match Prandtl numbers,

$$\frac{P_{rms}}{q} = f_4\ (r^*,\ R,\ M). \tag{5}$$

The power spectral density is determined as:

$$G = \int_{-\infty}^{\infty} \underset{t_o \to \infty}{\text{limit}}\ \frac{1}{t_o}\int_o^{t_o} p(r,t)p(r,t+\tau)dt\ \ e^{i2\pi f\tau}d\tau, \tag{6}$$

then

$$\frac{GU}{q^2L} = \int_{-\infty}^{\infty} \underset{t_o \to \infty}{\text{limit}}\ \frac{1}{t_o}\int_o^{t_o} \frac{p(r,t)p(r,t+\tau)}{q^2}\ \ e^{i2\pi\left(\frac{fL}{U}\right)\left(\frac{\tau U}{L}\right)}d\left(\frac{\tau U}{L}\right) \tag{7}$$

where L is the same characteristic length as used in the Reynolds number and in normalizing the coordinates.

Equations 1 and 7 imply that

$$\frac{GU}{q^2 L} = f_5 \left(\frac{fL}{U}, r^*, R, \bar{P}, \bar{G}, E\right), \tag{8}$$

and with the same arguments as stated for P_{rms},

$$\frac{GU}{q^2 L} = f_6 \left(\frac{fL}{U}, r^*, R, M\right). \tag{9}$$

Equations 5 and 9 then represent the scaling relationships for fluctuating pressure intensity and the pressure power spectral density.

Scaling with Incomplete Similitude

Unfortunately, the scaling laws of the preceeding section contain the common problem of modeling simultaneously with Reynolds and Mach numbers. Using only one gas, normally air, it is difficult to obtain large variations in fluid properties between model and prototype. That is:

$$\begin{aligned} a_m &\simeq a_p \\ \rho_m &\simeq \rho_p \\ \mu_m &\simeq \mu_p. \end{aligned} \tag{10}$$

The Reynolds and Mach scaling requirements are:

$$\frac{U_m}{a_m} = \frac{U_p}{a_p}$$

$$\frac{\rho_m U_m L_m}{\mu_m} = \frac{\rho_p U_p L_p}{\mu_p} \tag{11}$$

and, equations 10 and 11 lead to the conditions:

$$\begin{aligned} U_m &\simeq U_p \\ L_m &\simeq L_p. \end{aligned} \tag{12}$$

Obviously, the last equation prohibits the use of wind tunnel models that are

significantly smaller than the prototype for exact or nearly exact scaling. This unfortunate situation leaves several possible alternatives, for which applicability must be demonstrated experimentally or theoretically.

It is possible that the scaling is separable, or approximately so, such that for the shock conditions:

$$\frac{G_{\text{shock}}\, U}{q^2 L} = F_1\left(\frac{fL}{U}\right) F_2(R) F_3(M), \tag{13}$$

and the fluctuating pressure level would separate similarly.

Another possibility is that one of the effects will be insignificant compared to the other over some significant range. In that case, scaling can often be accomplished. Also, it is sometimes possible to artificially simulate one of the effects, for example, the Reynolds effect has sometimes been approximated with increased surface roughness. The success of this generally depends on the strength of the effect in the range being tested. That is, the test would likely be representative if the Reynolds effect were weak in the test-prototype range, but if there were a strong Reynolds effect on the quantity being tested, the results would be much more questionable.

Another possibility is the development of an analytical model. Even though the complexities of the flow field seem to preclude the direct solution of the governing equations in complete form, a semi-empirical model can be extremely helpful for data extrapolation, providing that the model is stated in terms of Mach and Reynolds effects which are known or can be determined. For this purpose, the results are tied to experimental data at points so that the model need only to represent trends reasonably.

All statements, up to this point, assume air to be the test gas. Another possibility is to use a gas with properties such that:

$$\frac{a_m \rho_m}{\mu_m} \gg \frac{a_p \rho_p}{\mu_p} \tag{14}$$

since this leads to:

$$L_m << L_p. \tag{15}$$

The success here, obviously depends on the identification and availability of such a gas. In the use of different gases one should be on guard for specific heat effects.

The last, and most difficult to delineate case, is scaling with incomplete geometric similarity. It is difficult to discuss because it involves experience and intuition to a major degree. For example, it is intuitive that a protuberance, which is buried in a separated region, will have little effect on the balance of the flow field, whereas a protuberance ahead of a separation shock will alter the flow significantly. Continuing this train of thought, one concludes that scaling should be possible if the significant geometry and parameters are matched, even though there may be considerable mismatching of insignificant geometry and parameters. This type of argument is always implicit whenever data are compared between separations produced by different geometries, particularly if a comparison is made, or suggested, between a separation produced by a rigid surface and a separation produced by a gaseous plume.

If one considers the application of equation 9 to the pressure under a separation shock ($r^* = r^*_{shock}$), and has overcome the obstacles stemming from lack of complete geometric similarity, then:

$$\frac{G_{shock}\, U}{q^2 L} = F_4 \left(\frac{fL}{U}, \frac{\rho UL}{\mu}, \frac{U}{a}\right), \tag{16}$$

and the next task is to select the most representative values for the variables involved. This is never a problem with complete similarity; only consistency between the model and prototype is required. However, with incomplete geometric similarity, identification of the most pertinent variables

is essential if any success is to be achieved.

In equation 16 several variables may be identified readily. The velocity, dynamic pressure, and speed of sound should be taken outside the boundary layer just upstream of the shock wave. Freestream values may be used only if they are essentially the same. It is not as clear where the viscosity should be taken. However, considering the similarity of turbulent boundary layers, it probably can be taken outside the boundary layer providing that thermal boundary conditions at the surface are reasonably matched. The variable that is least obvious is the one directly associated with geometry: the length. Clearly, it must be characteristic of some flow feature, and obvious candidates are a boundary layer thickness and separation length. (Again, if boundary layer similarity is reasonably maintained, it doesn't matter which boundary layer thickness is selected.) Without complete similarity, it is even possible that more than one length is characteristic so that

$$\frac{G_{\text{shock}}\, U}{q^2 L} = F_5\left(\frac{fL}{U}, \frac{L_1}{L}, \frac{\rho UL}{\mu}, \frac{U}{a}\right), \tag{17}$$

where L is either the boundary layer thickness or the separation length, and L_1 is the other. However, it is likely that with the best choices for the variables involved, a much simpler relationship than that indicated by equation 17 is possible. To consider a few possibilities, assume that the only significant Reynold's effect is reflected by the boundary layer thickness, δ, and that the only significant Mach effect is reflected by the separation length $\bar{x}$. Then equation (17) would reduce to:

$$\frac{G_{\text{shock}}\, U}{q^2 \bar{x}} = F_6\left(\frac{f\bar{x}}{U}, \frac{\bar{x}}{\delta}\right) \tag{18}$$

since the Reynolds and Mach effects would be indirectly accounted for by the

lengths. What seems more likely, is that the Mach effect would be reflected in the shock angle, θ, since it is directly related to shock strength. Then one might have:

$$\frac{G \text{ shock } U}{q^2(\bar{x} \text{ or } \delta)} = F_6 \left(\frac{f(\bar{x} \text{ or } \delta)}{U}, \theta\right) \tag{18}$$

Of course, the ultimate simplicity would result in identifying a single length which reflected both the essentials of the Mach and Reynolds effect, so that:

$$\frac{G \text{ shock } U}{q^2_L} = F_8 \left(\frac{fL}{U}\right) \tag{20}$$

Using the form of equation 20, Robertson [9] shows good correlation for the shock spectra generated by a 45^o wedge at Mach 2, and cylindrical protuberances at Mach 1.4 and 1.6, using separation length as significant. The present shock data for plume induced separation at Mach 2.9 do not correlate quiet as well, but do correlate slightly better with separation length than with boundary layer thickness. (See Figure 16.) It is not clear whether the differences arise from incomplete similarity or from a plume induced separation as compared with separation for a rigid corner. More data, over a range of conditions, would be helpful in identifying the simplest reliable scaling laws.

MISCELLANEOUS

Transducer Effect

Fluctuating pressure data reported were taken with a 2 mm diameter strain gage type transducer, whereas similar data have been previously taken with a 5 mm diameter piezoelectric type transducer [7]. A comparison of the resulting power spectra is given in Figure 17. Unfortunately, there are extraneous conditions involved which preclude the conclusion that the difference is due solely to transducer effect. The data taken with the 2 mm transducer were processed as described previously in this paper, whereas the data from the 5 mm transducer

were processed by recording it on magnetic tape, making a continuous loop of about 15 seconds of run, and scanning that signal with a continuously variable bandwidth filter keyed to the one-third octave distribution. The resulting output exhibited considerable scatter and was faired with a smooth curve before processing into a power spectrum. By all indications, however, the present data should be more reliable since it involves no interpretation and is taken with a smaller transducer.

Harmonic Effects

Figure 18 illustrates a power spectrum with a high level of plume unsteadiness at a low frequency. A secondary spike is obvious at twice the frequency of the primary spike (and consequently at twice the forcing frequency). This is evidently a harmonic effect, and in fact, careful inspection of the spectrum will identify small spikes at four-times and eight-times the forcing frequency. This effect is evident only in spectra associated with low frequency forcing, but presumably, it is present in other cases with the effects obscured by the larger bandwidths characteristic of the one-third octave spectrum at higher frequencies.

CONCLUDING REMARKS

Several effects associated with plume induced flow separation have been identified. The following statements are applicable over the range of this study.

1. The separation shock exhibits an excursion about some mean location and maintains essentially constant direction as it moves. This is true with or without plume unsteadiness.

2. The probability that the separation shock is located in a given position interval at a given instant is not influenced by plume unsteadiness.

3. Periodic plume unsteadiness produces a spike on the separation shock surface pressure power spectrum. The spike strength is proportional to the plume pulsing magnitude. The proportionality is constant over a frequency range.

4. The broadband level of the separation shock surface pressure fluctuations is not affected by periodic plume unsteadiness, so that the spectrum spike is produced at the expense of the balance of the spectrum.

5. Periodic plume unsteadiness produces secondary spikes in the separation shock pressure spectrum at higher octaves of the forcing frequency. Although the spike magnitudes are small compared to the primary spike, they have been observed at frequencies up to three octaves above the forcing frequency.

6. Separation shock activity is reduced by the pressure of a lateral surface protuberance which extends partially through the boundary layer. The shock excursions are restricted, and the shock root-mean-square pressure is reduced.

7. Exact scaling the statistics of pressure fluctuations between similar bodies of greatly different size is difficult because of conflicting

requirements for Reynolds and Mach similarity. It may be possible to identify flow field dimensions which reflect the Reynolds and Mach effects for successful approximate scaling, but this would require a reliable phenomenological model and/or sufficient data for assurance.

8. The separation shock spectra reported agree slightly better with protuberance and compressions corner shock data if separation length is taken as characteristic, as opposed to boundary layer thickness.

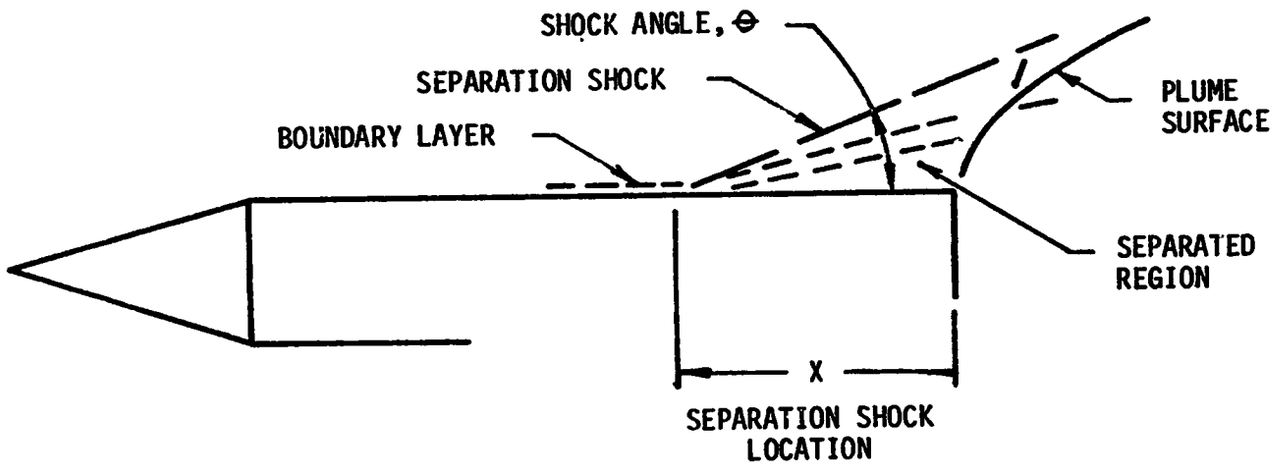

Figure 1. Plume Induced Flow Separation

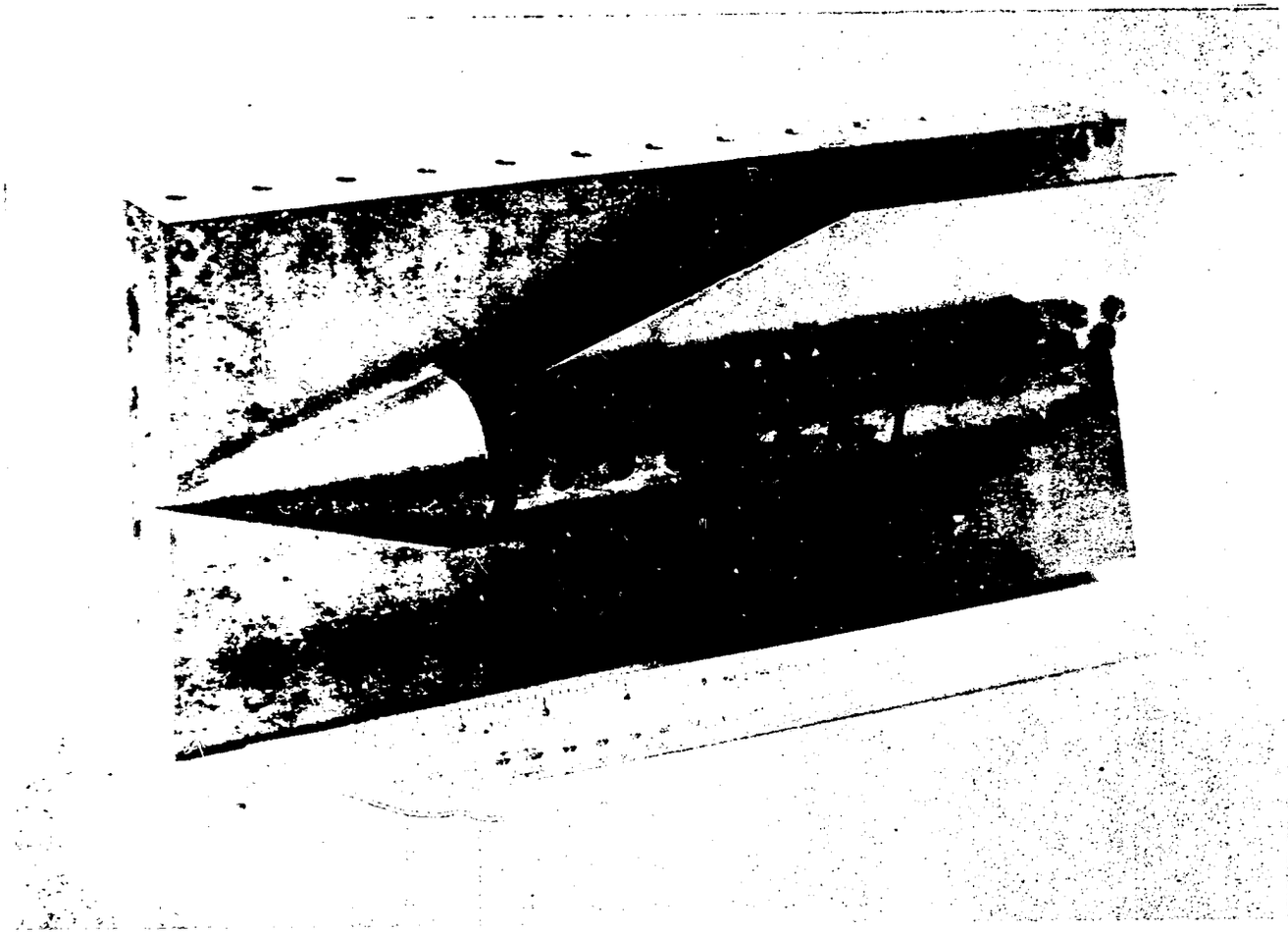

Figure 2. Photograph of the Test Model

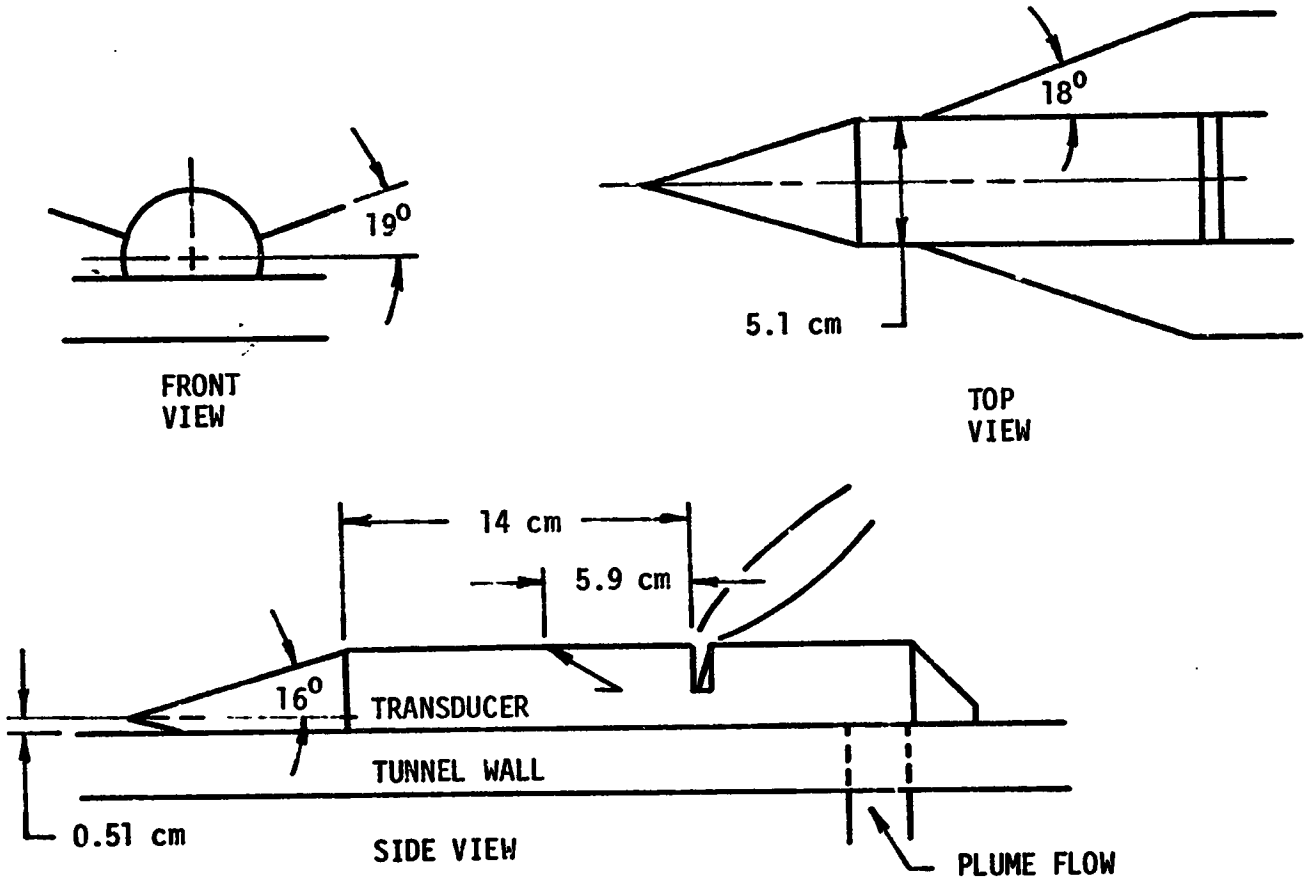

Figure 3. Details of the Test Model

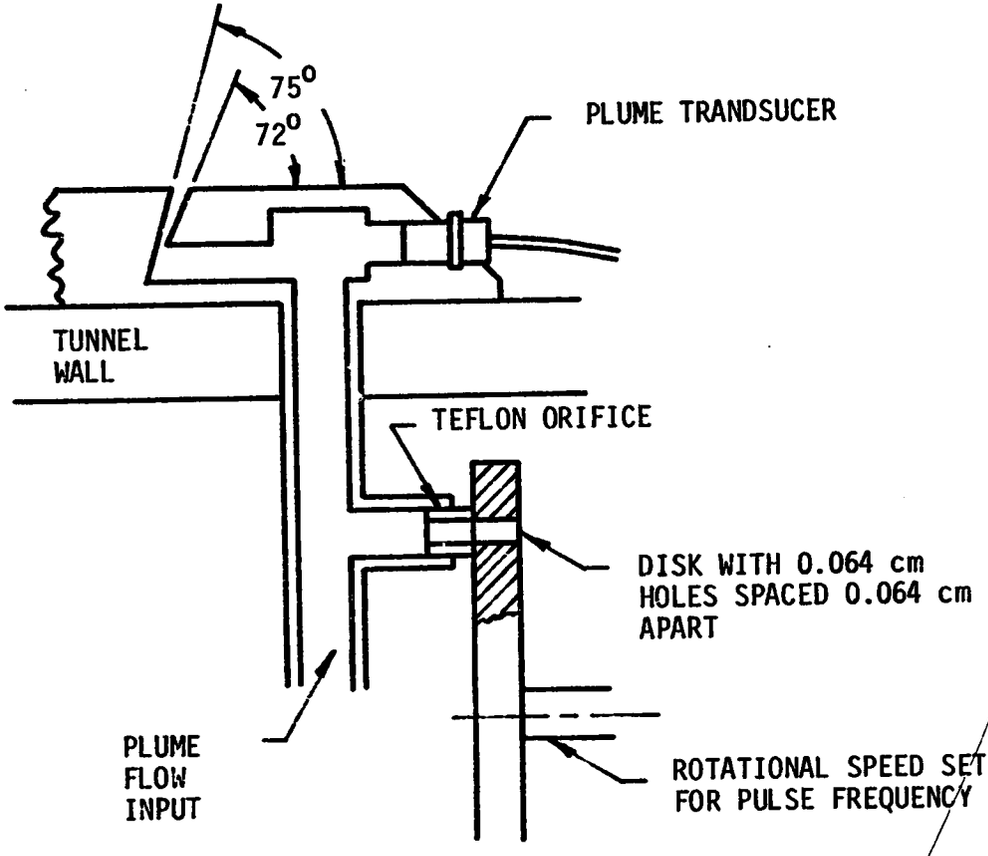

Figure 4. Plume Generation Details

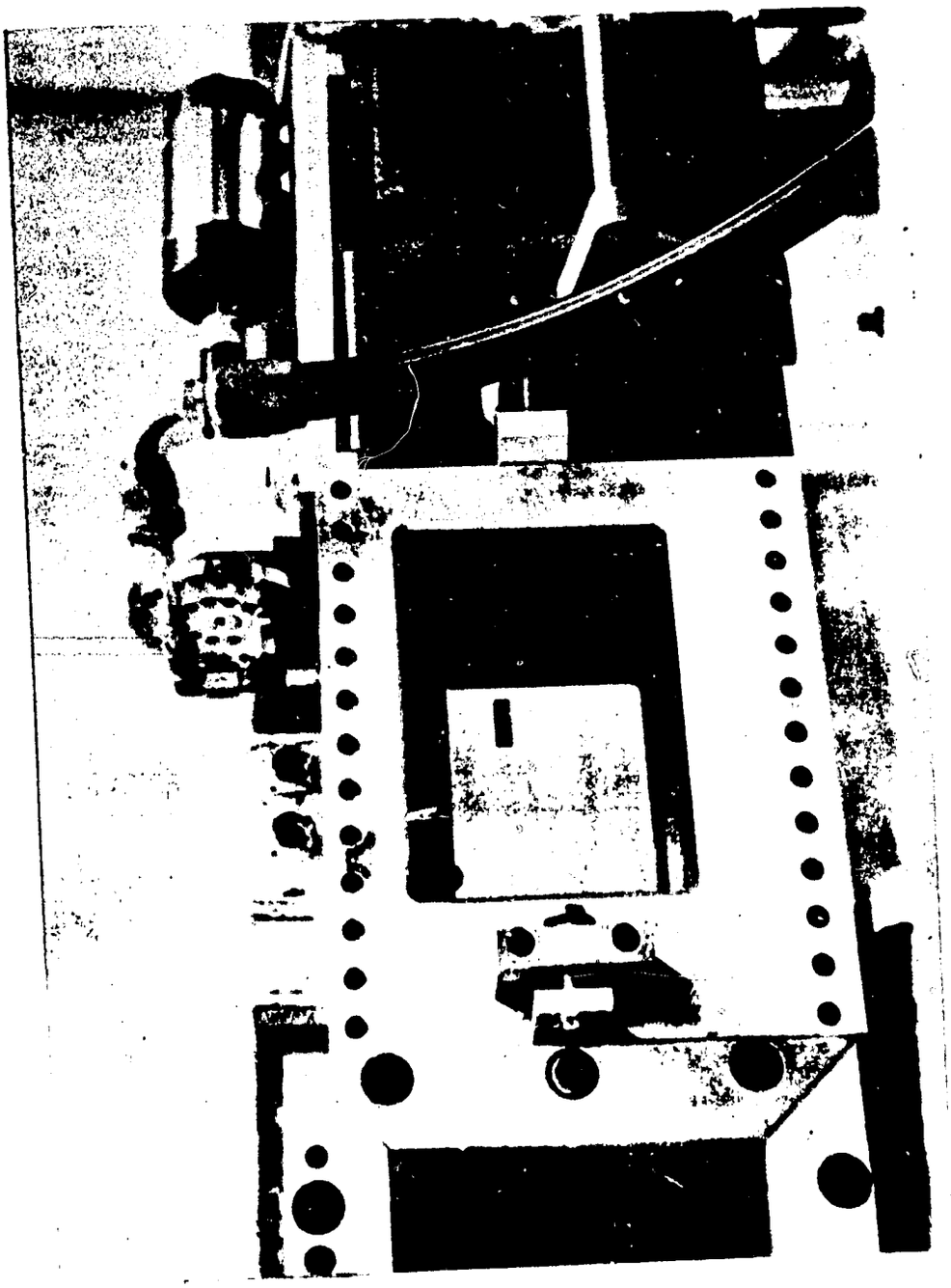

Figure 5. Plume Pulsing Apparatus

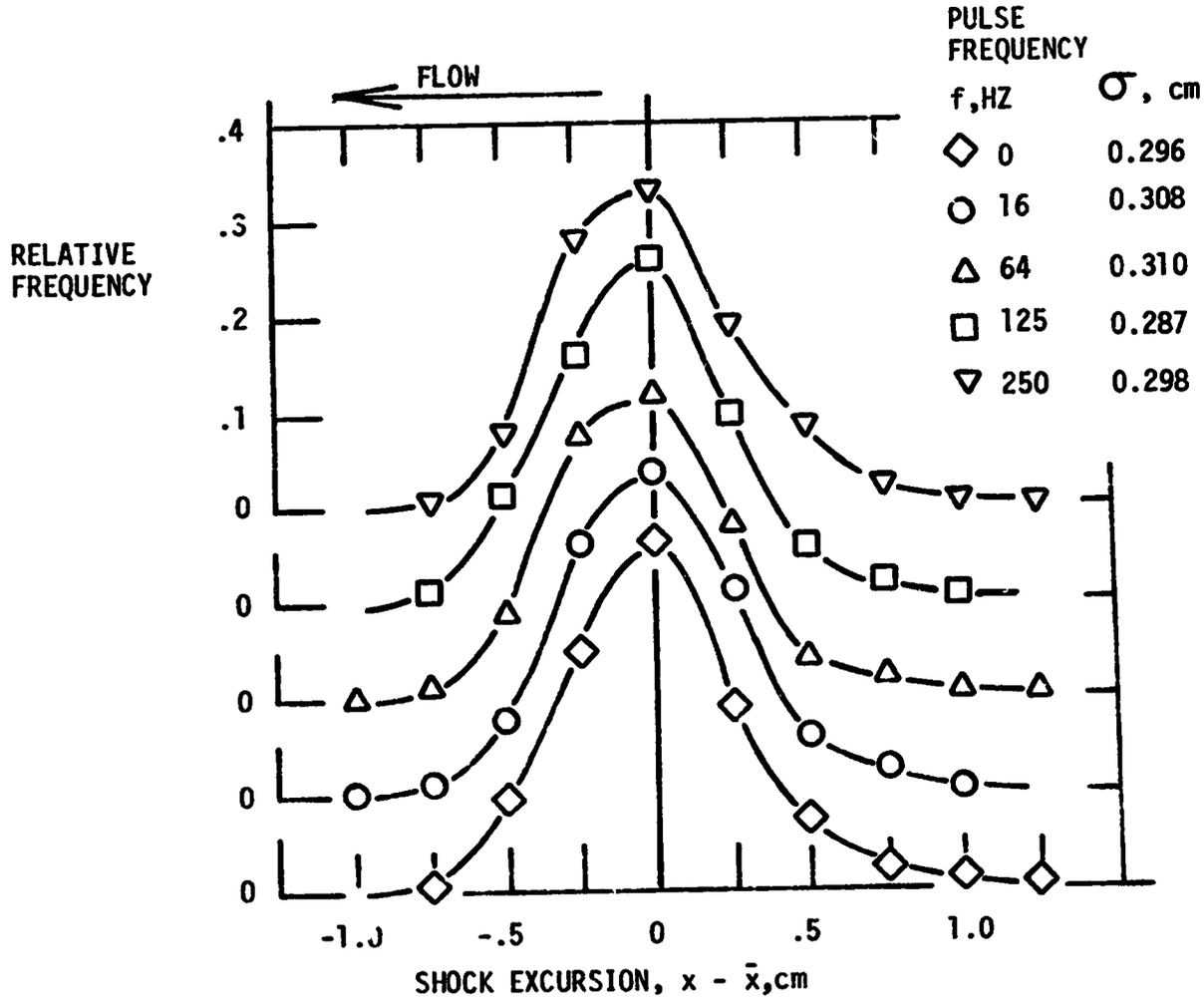

Figure 6. Separation Shock Excursions,
With and Without Periodic Plume Unsteadiness

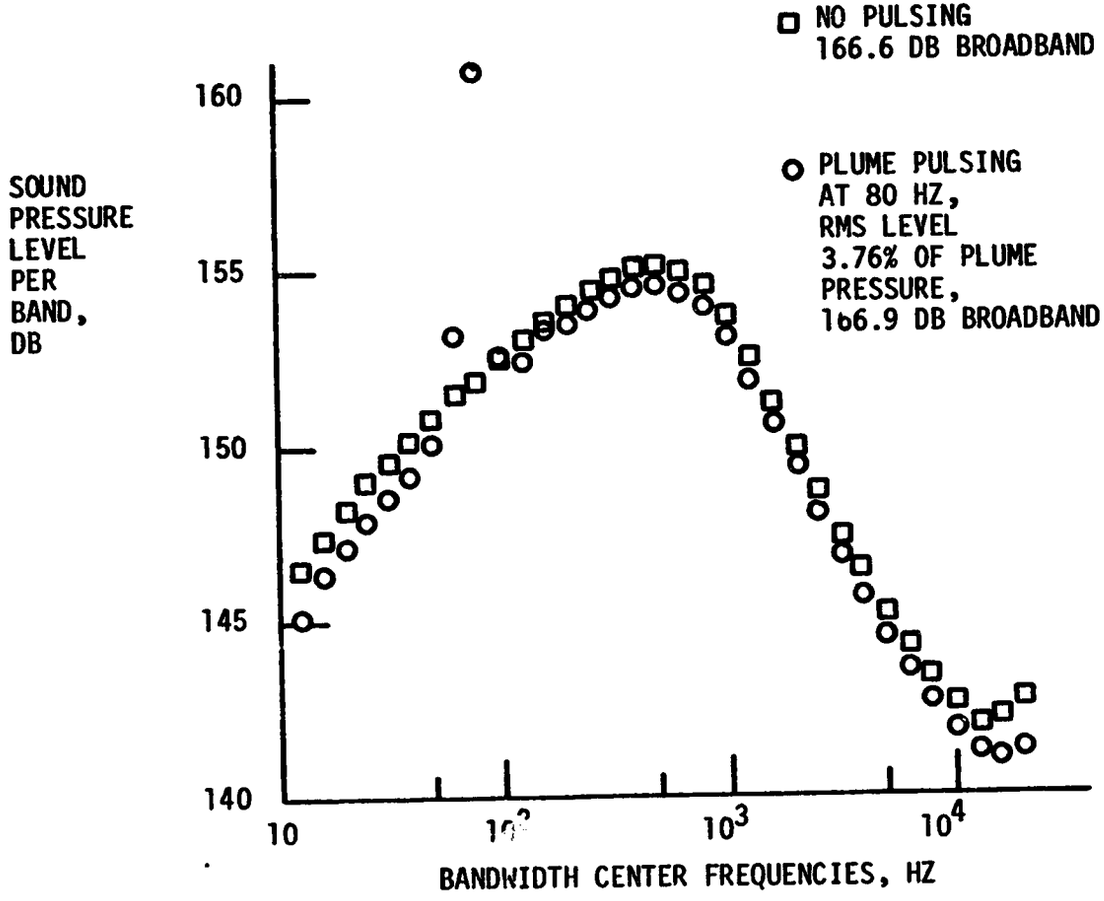

Figure 7. One-Third Octave Raw Separation Shock Spectra, With and Without Periodic Plume Unsteadiness

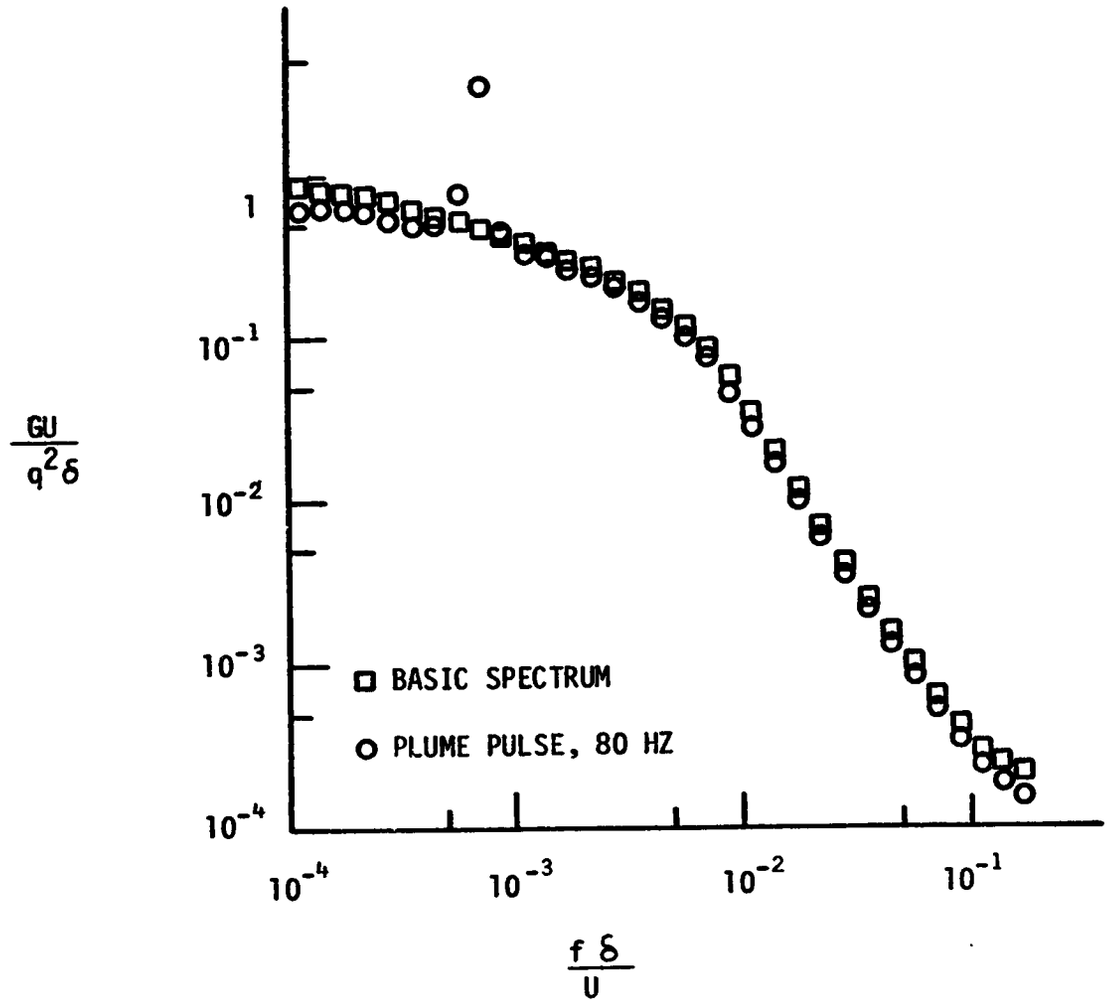

Figure 8. Separation Shock Power Spectra, With and Without Plume Unsteadiness

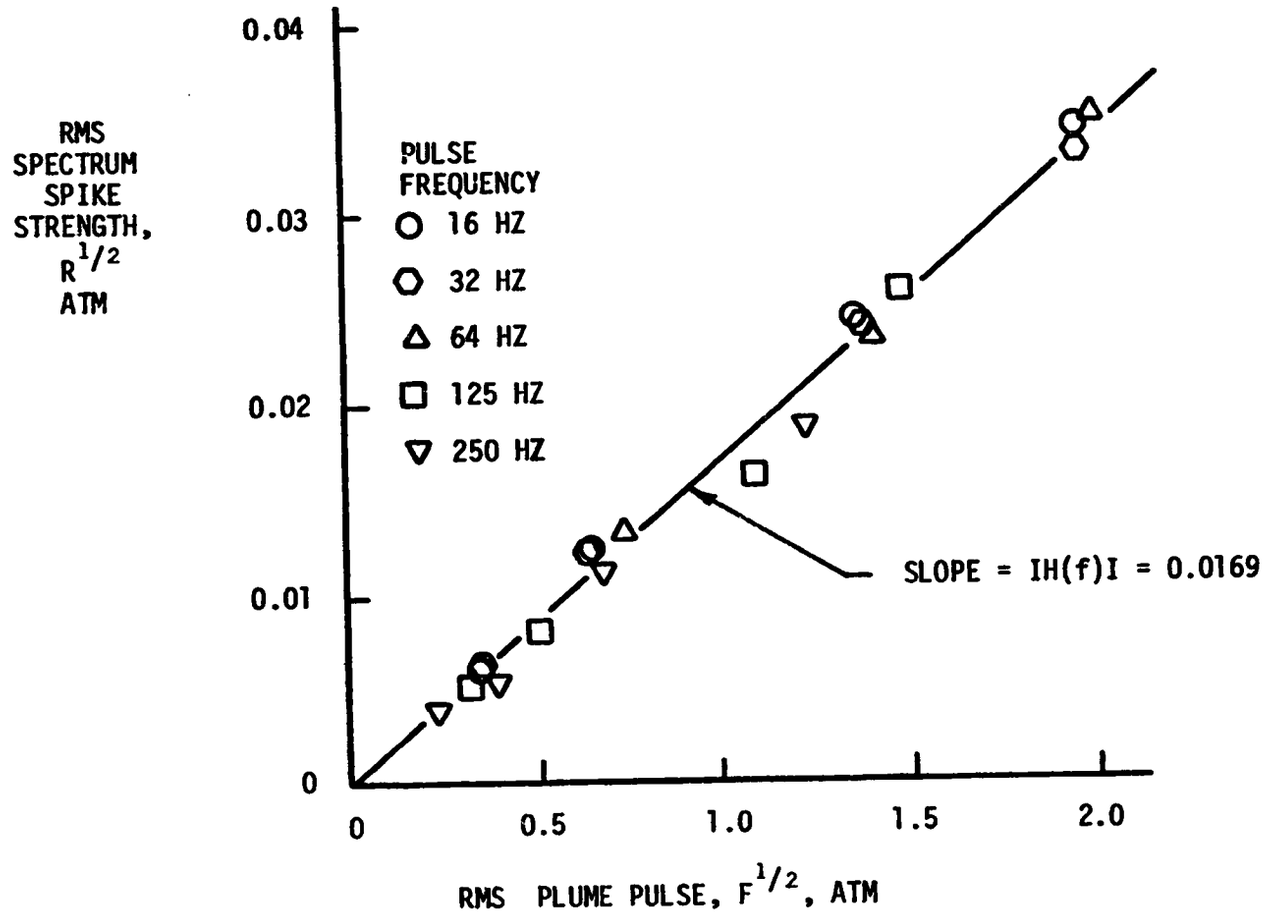

Figure 9. Power Spectrum Response to Periodic Plume Unsteadiness

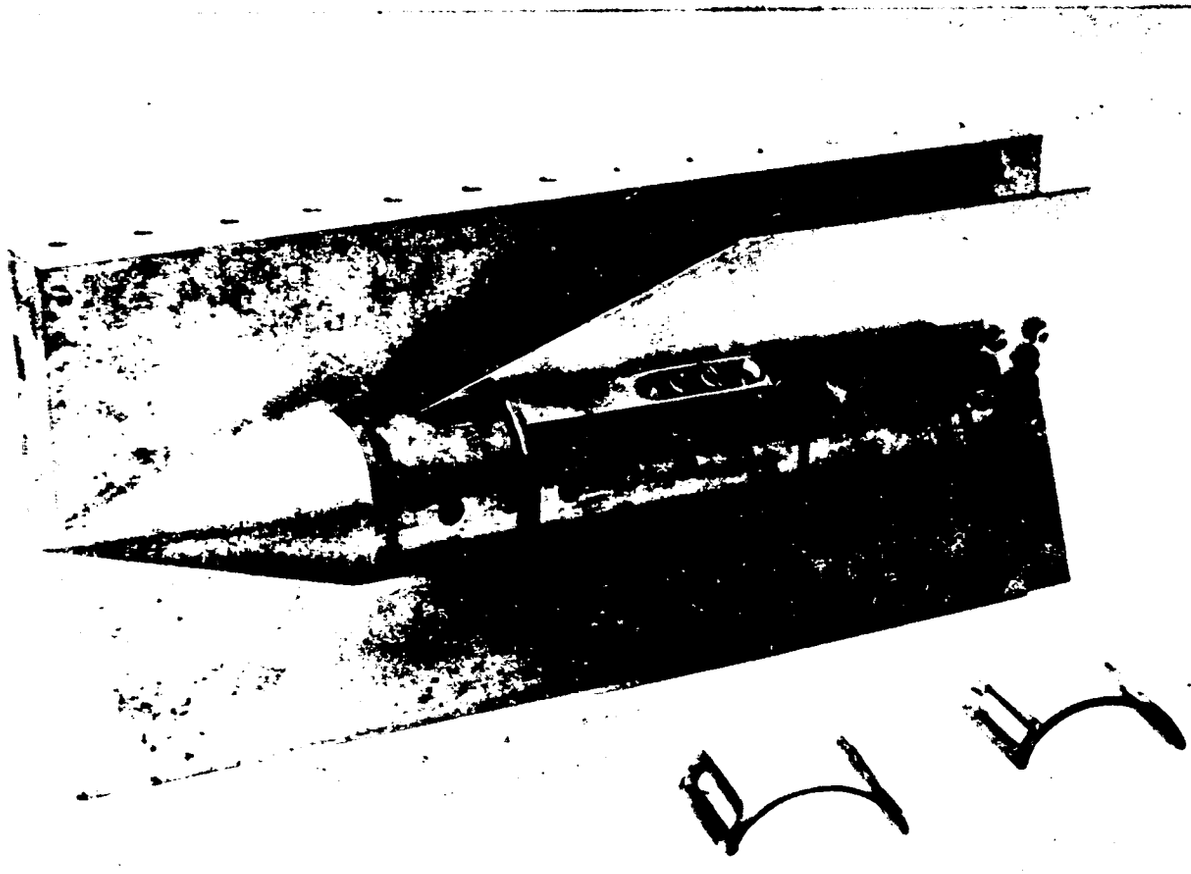

Figure 10. Test Model Configuration for Shock Stabilization Tests

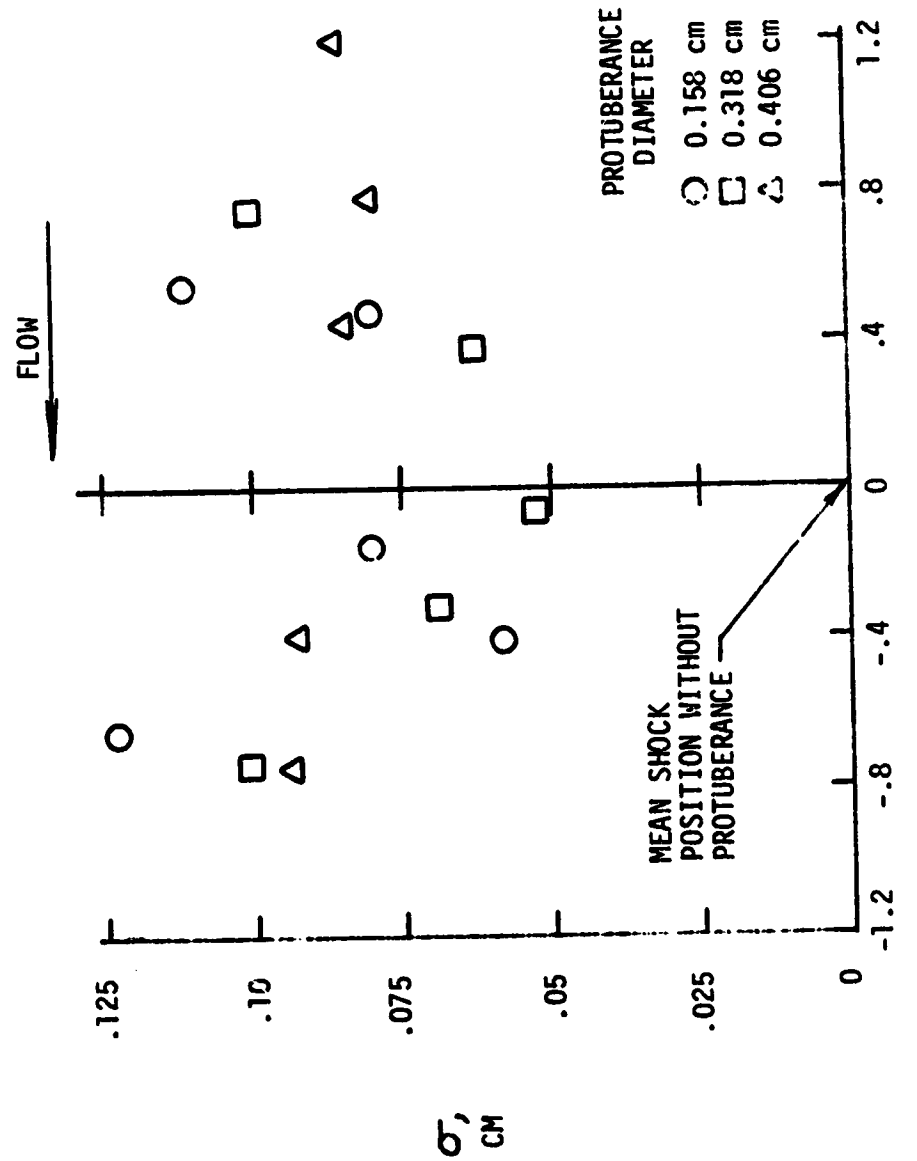

Figure 11. Standard Deviation of Separation Shock Movement for Different Protuberance Locations

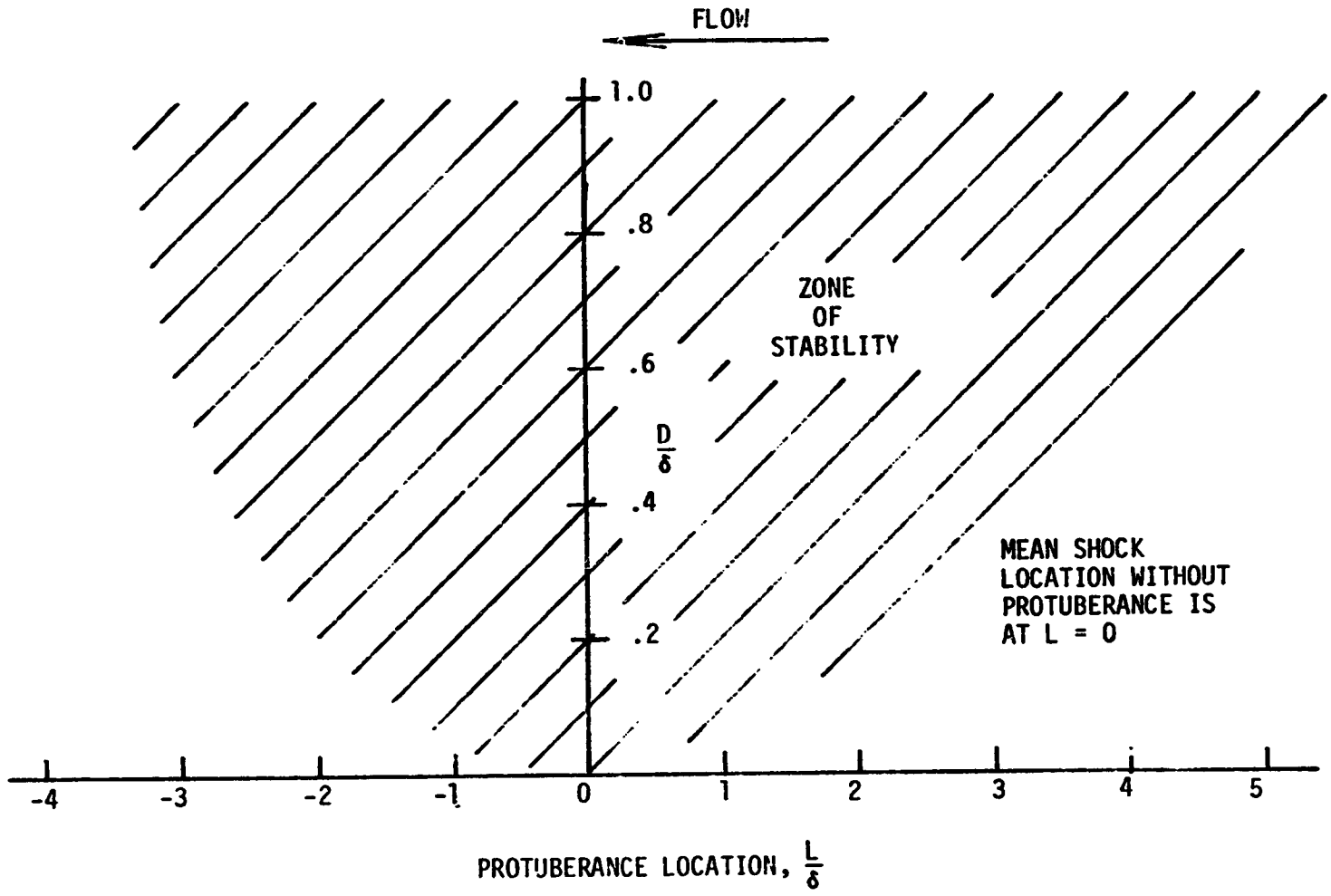

Figure 12. Zone of Separation Shock Stabilization for Circular Protuberances

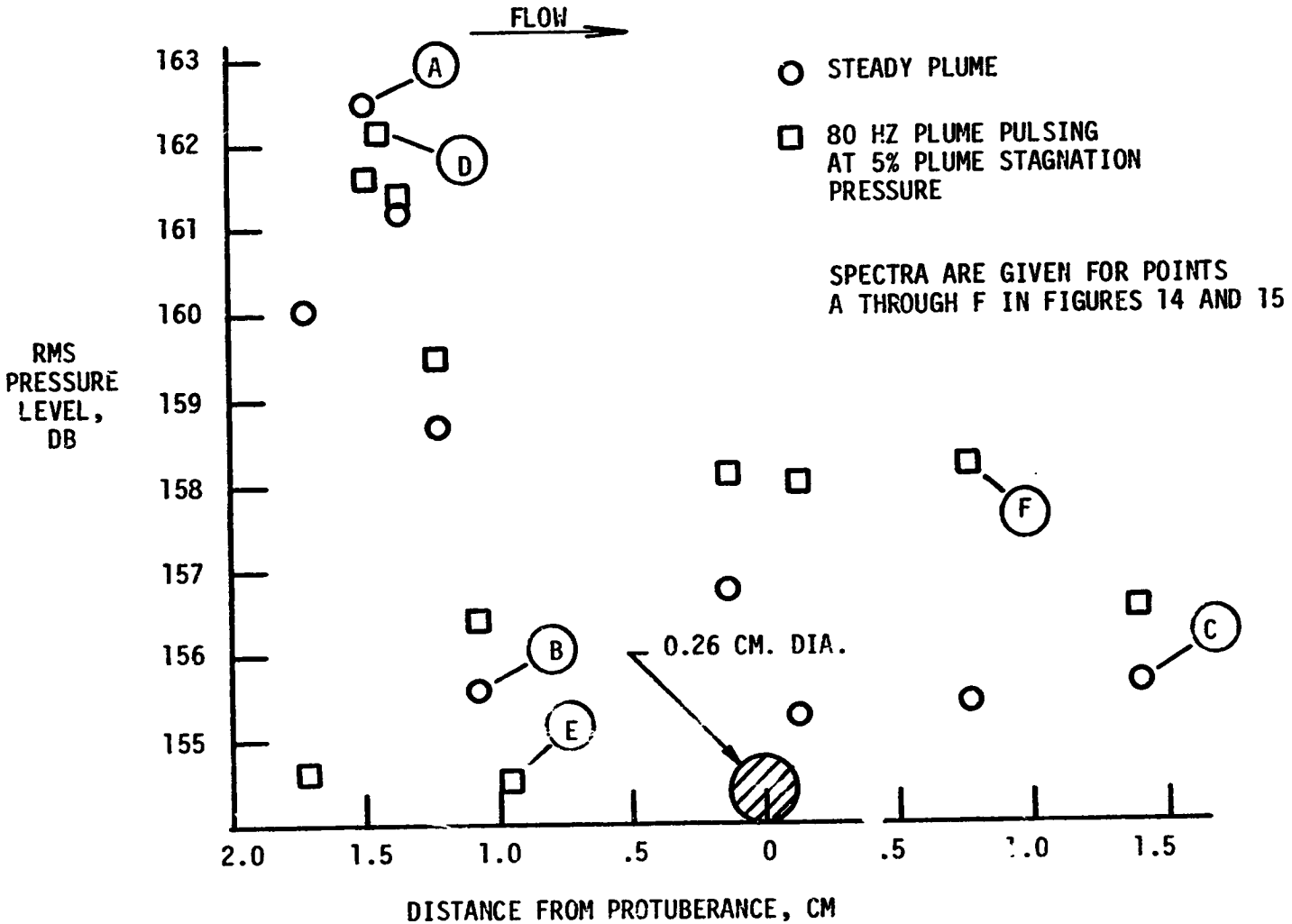

Figure 13. RMS Pressure Levels Near a Circular Protuberance, With and Without Plume Unsteadiness

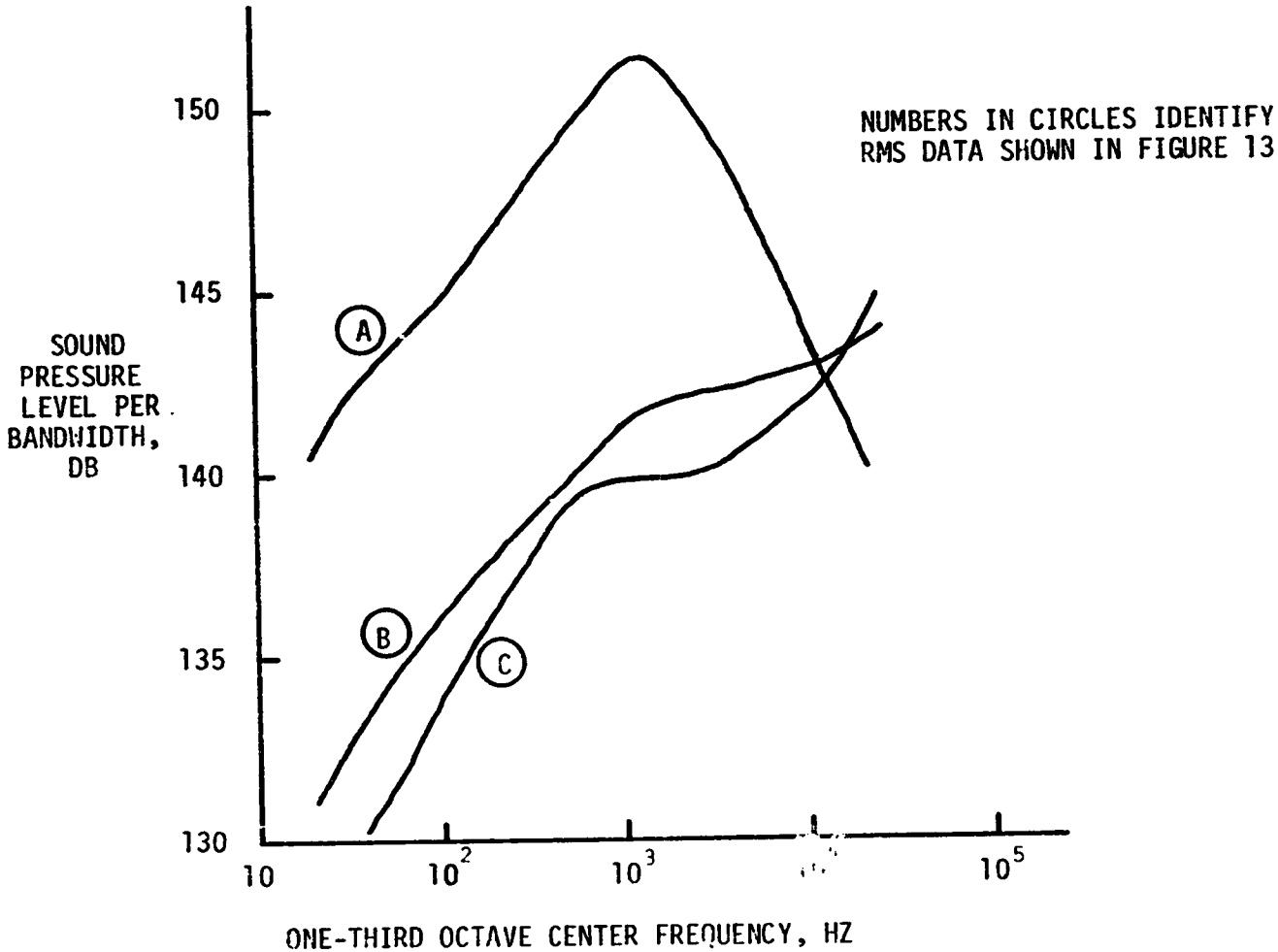

Figure 14. One-Third Octave Raw Spectra for Locations Near a Circular Protuberance, Steady Plume

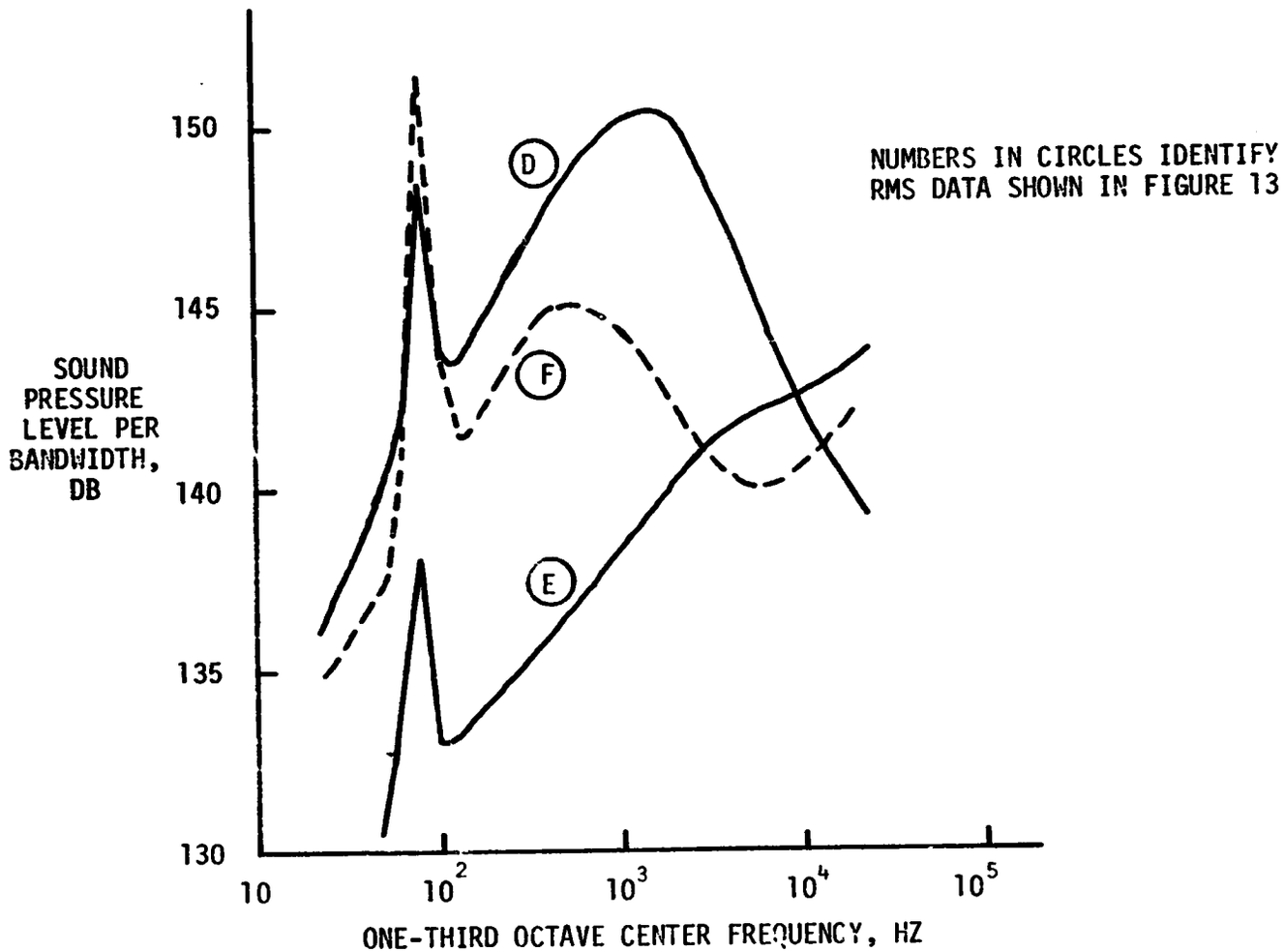

Figure 15. One-Third Octave Raw Spectra for Locations Near a Circular Protuberance, 80 Hz Plume Pulsing

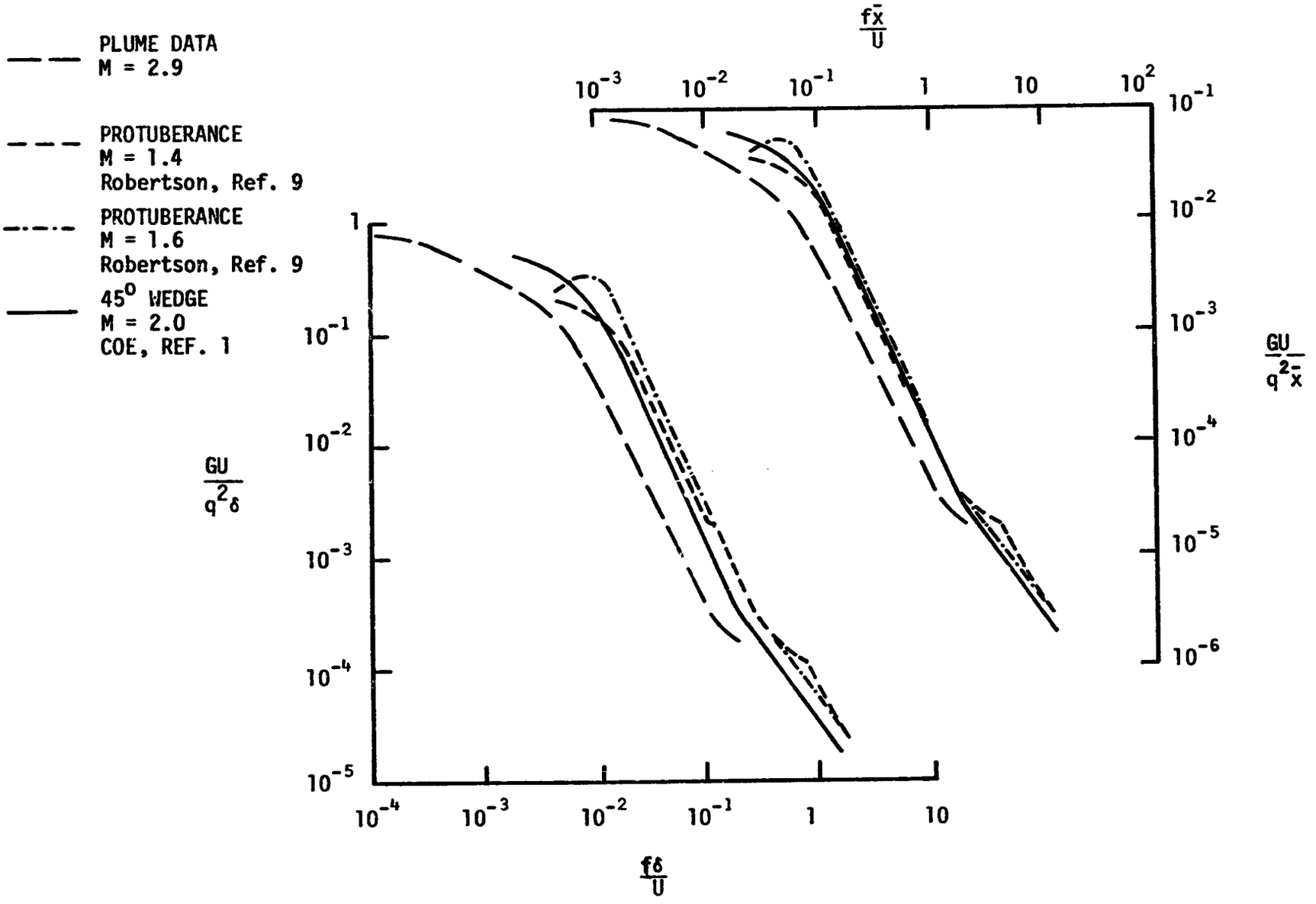

Figure 16. Comparison of Spectra Normalized with Boundary Layer Thickness and with Separation Length

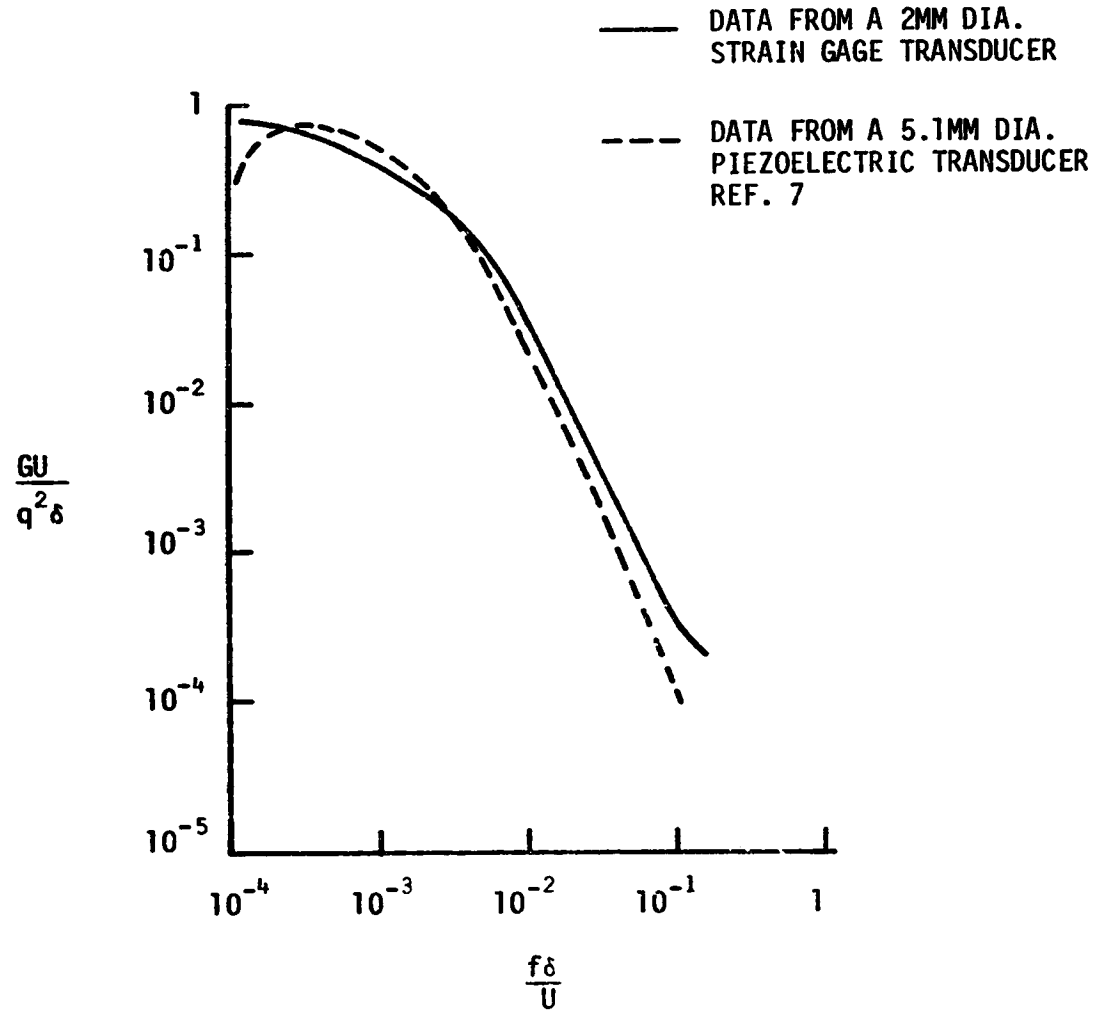

Figure 17. Comparison of Spectra Produced by Different Pressure Transducers

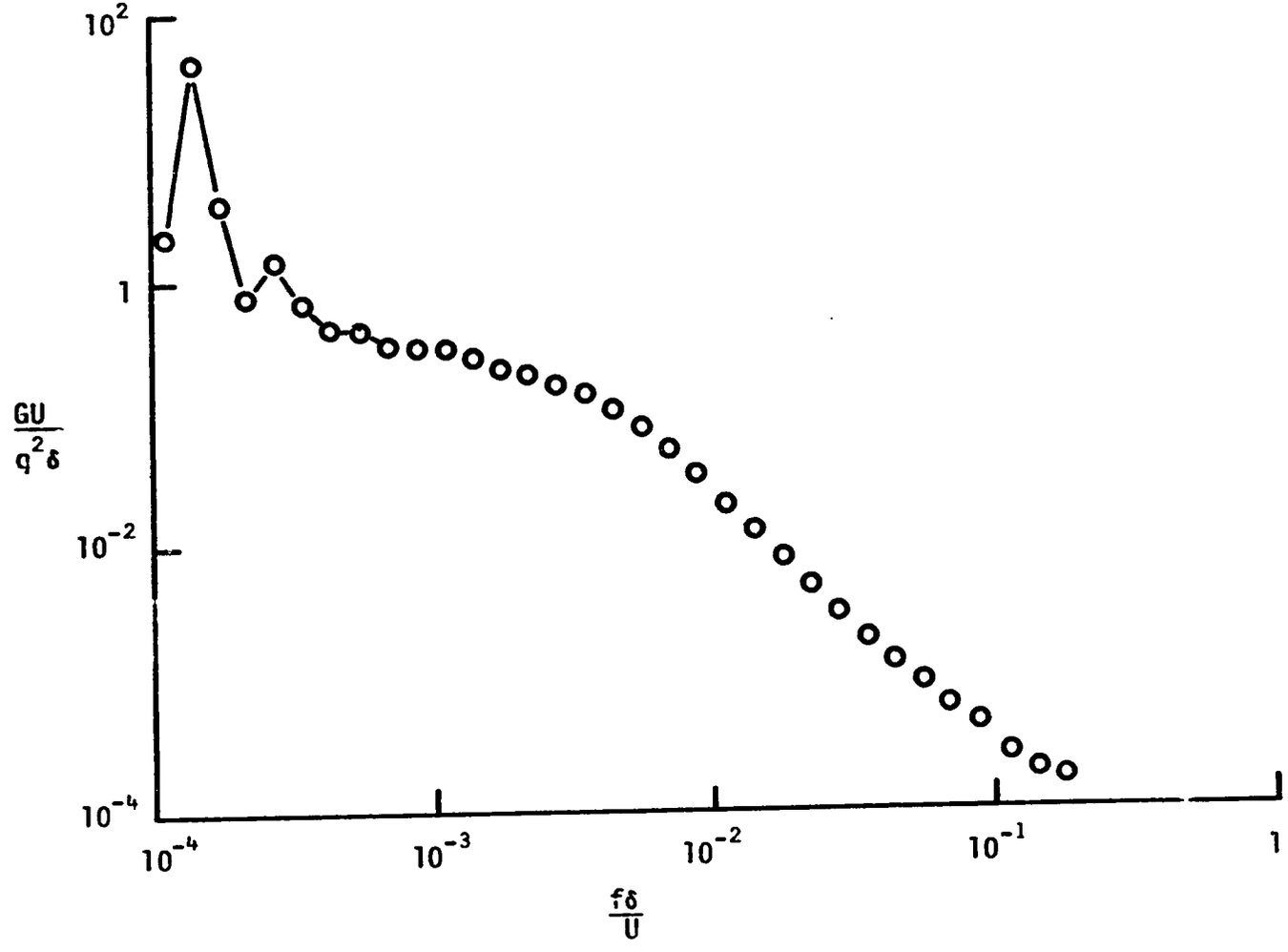

Figure 18. Power Spectrum Exhibiting Harmonics from Plume Pulsing at 16 Hz

LIST OF REFERENCES

1. Coe, C.F.: Surface-Pressure Fluctuations Associated with Aerodynamic Noise. NASA SP-207, 1969, pp. 409-424.

2. Coe, C.F. and Chye, W.J.: Pressure-Fluctuation Inputs and Response of Panels Underlying Attached and Separated Supersonic Turbulent Boundary Layers. NASA TM X-62, 189, 1972.

3. Kistler, A.L.: Fluctuating Wall Pressure Under a Separated Supersonic Flow. J. Acoust. Soc. Am., Vol. 36, No. 3, 1964, p. 543.

4. Trilling, L.: Oscillating Shock Boundary-Layer Interactions. J. Aero. Sci., May 1958, pp. 301-304.

5. Jones, J.H.: Acoustic Environmental Characteristics of the Space Shuttle. Proc. Space Shuttle Technology Conf., July 1970.

6. Boggess, A.L., Jr. and Doughty, J.O.: An Investigation of the Unsteady Flow Associated with Plume Induced Flow Separation. Bureau of Engineering Research Report No. 149-02, The University of Alabama, Tuscaloosa, 1972.

7. Doughty, J.O.: Effects of Periodic Plume Pulsing on the Flow Field Generated by Plume Induced Flow Separation. Bureau of Engineering Research Report No. 164-02, The University of Alabama, 1973.

8. Schlichting, H.: "Boundary Layer Theory, 6th Ed.", McGraw-Hill Book Co., New York, 1968.

9. Robertson, J.E.: Prediction of In-Flight Fluctuating Pressure Environments Including Protuberance Induced Flow. Wyle Laboratories Report WR 71-10, 1971.